Mechanism and reaction coordinate of directional charge separation in bacterial reaction centers

Eisenmayer, T.J.; Groot, H.J.M. de; Wetering, E. van de; Neugebauer, J.; Buda, F.

THE JOURNAL OF PHYSICAL CHEMISTRY Letters

Letter

pubs.acs.org/JPCL

Mechanism and Reaction Coordinate of Directional Charge Separation in Bacterial Reaction Centers

Thomas J. Eisenmayer,[‡] Huub J.M. de Groot,[‡] Elbert van de Wetering,[‡] Johannes Neugebauer,[†] and Francesco Buda*[,‡]

[‡]Leiden University, Leiden Institute of Chemistry, Einsteinweg 55, P.O. Box 9502, 2300 RA Leiden, The Netherlands

[†]Technical University Braunschweig, Institute for Physical and Theoretical Chemistry, Hans-Sommer-Str. 10, 38106 Braunschweig, Germany

Supporting Information

ABSTRACT: Using first-principles molecular dynamics, we predict the reaction coordinate and mechanism of the first charge-separation step in the reaction center of photosynthetic bacteria in a model including the special pair (P) and closest relevant residues. In the ground state, a dynamical localization of the highest occupied orbital is found to be a defining characteristic of P. This feature is linked to the tuning of the orbital energy levels by the coupling with two collective low-frequency vibrational modes. After electronic excitation, we demonstrate one specific mode that couples to P*, representing the reaction coordinate along which the excited state develops. The characteristic vibrational coordinate we predict to be the rotation of an axial histidine (HisM202), which selectively lowers the energy of one (P_M) of the two bacteriochlorophylls in P. This leads to a unidirectional displacement of electron density to establish $P_L^+P_M^-$ charge-transfer character, a hypothesis well-supported by an extensive framework of experimental evidence.

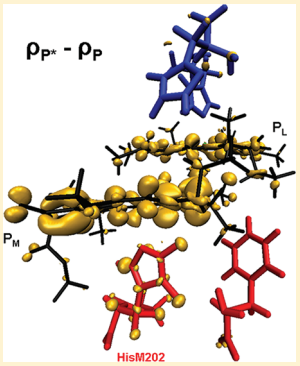

SECTION: Biophysical Chemistry

Low-frequency collective modes of the special pair (P) are known to remove the barrier for charge separation in photosynthetic bacteria along a structurally unknown reaction coordinate.[1] In the pseudosymmetric architecture of photosynthetic reaction centers (RCs), charge separation occurs preferentially along one (L) of two cofactor branches. Numerous experiments find vibrational modes in the region 100−150 cm^{-1} that strongly couple to the initial photoexcited state P*.[2−4] On a 3 ps time scale the primary electron donor is oxidized and an accessory bacteriochlorophyll (B_L) is reduced.[5] The formation of the first L-branch photoproduct is coupled to a 130 cm^{-1} mode.[1] Stark experiments find an internal charge transfer (CT) character $P_L^+P_M^-$ to have most influence on P*.[6] The ground-state electron density distribution of P and of the radical cation $P^{\bullet+}$ is influenced by the immediate protein environment, as indicated by solid-state NMR, ENDOR/EPR, and density functional calculations.[7,8] The axial histidines are known to donate electron charge to bacteriochlorophyll chromophores in both RCs and light-harvesting complexes, and the acetyl group conformation tunes the energy of the π-conjugated bacteriochlorophylls planes.[9,10]

We report ab initio molecular dynamics (AIMD) simulations[11,12] at room temperature of a model including the special pair and the relevant closest protein environment (Figure 1). Long-range interactions are not included in the model, but the chosen residues are thought to be sufficient to capture the most important effects for the local dynamics. (See SI-1 in the Supporting Information for a test where long-range electrostatic interactions are included using a continuous model.) Within this approach, we directly observe how the dynamical evolution of the nuclear coordinates is coupled to the corresponding electronic structure rearrangement calculated with density functional theory (DFT). This allows us to predict the reaction coordinate of charge separation and the mechanism leading to the first CT intermediate.[13] For more details on the computational methods and model, see the Supporting Information (SI-1).

The ground-state trajectories show that frontier orbital (HOMO−LUMO) localization is a dynamical characteristic of the special pair at room temperature (Figure SI-2 of the Supporting Information). On a 1 ps time scale, the HOMO fluctuates from complete localization on one dimer half to intermediate delocalization to complete localization on the other dimer half. The LUMO shows the same dynamical behavior with opposite phase (Movie 1 in the Supporting Information); when the HOMO is localized on P_M, the LUMO is localized on P_L and vice versa.

This result can be interpreted by thermally induced orbital energy fluctuations of the two monomers: When the HOMO energy of P_L is lower than the HOMO energy of P_M, the HOMO of P shows an essentially monomeric character being localized entirely on P_L; when the orbital energies of the

Received: December 25, 2011
Accepted: February 21, 2012
Published: February 21, 2012

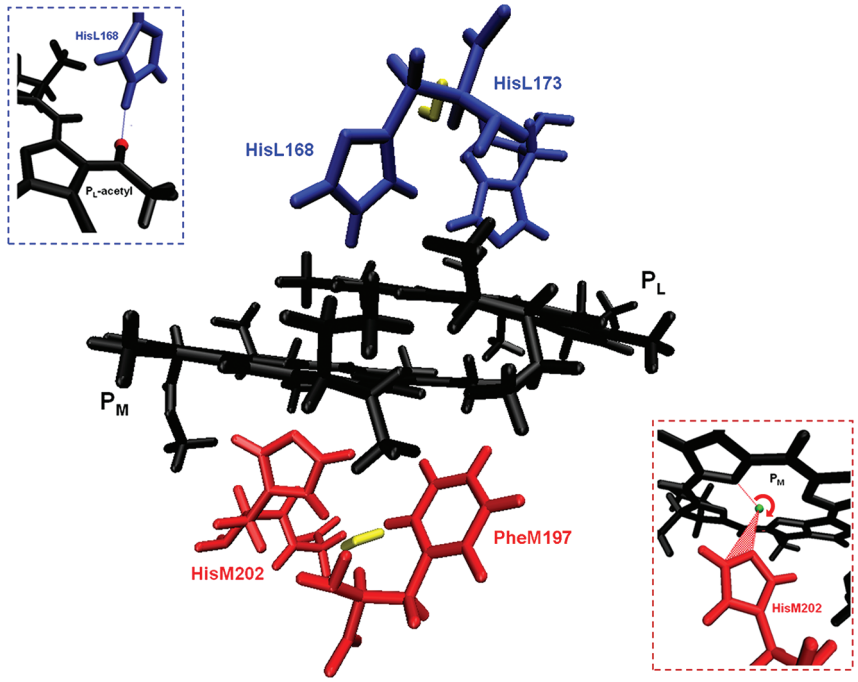

Figure 1. Model of the special pair and direct surroundings, including the axially coordinated histidines HisL173, HisM202, the water molecules in their vicinity and the residues HisL168 and PheM197. The protein environment mechanical constraints are ensured by fixing the tails of the histidines, the phenylene, and the truncated phytyl chains. Left top: hydrogen bond between HisL168 and the acetyl oxygen of the P_L dimer half. Right bottom: dihedral angle of the histidine ring of HisM202 with respect to the Mg−N_τ coordination axis.

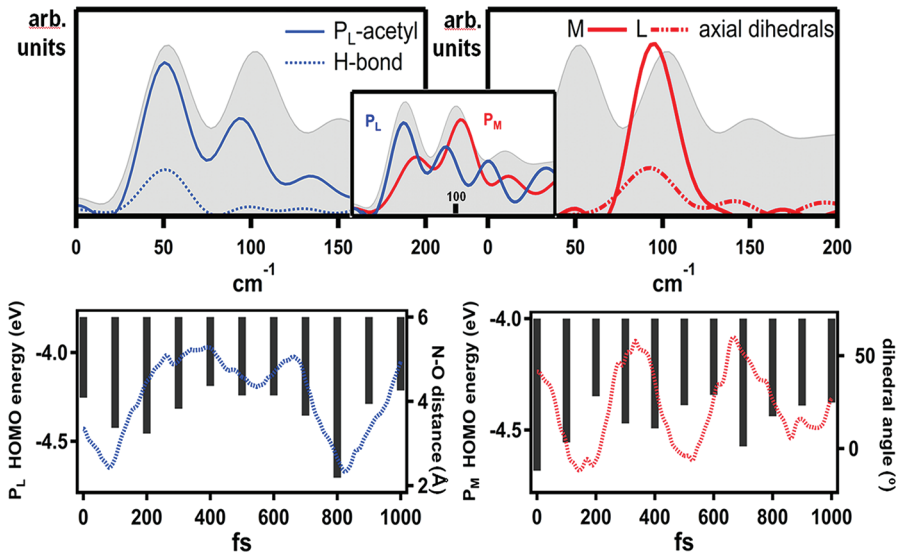

Figure 2. Total vibrational density of states (VDOS) obtained from the dynamical trajectory (gray shading top graphs). Blue lines in the top left represent conformational dynamics of the ∼50 cm^{-1} mode obtained from the time evolution of the hydrogen bond with HisL168 and of the P_L-acetyl group. The inset gives the VDOS for P_L in blue. The bottom left graph gives the hydrogen bond distance (blue line) with the P_L-HOMO energy (bars) in the time domain. Red lines represent conformational dynamics of the ∼100 cm^{-1} mode; the top right graph gives the VDOS obtained from the axial histidine dihedrals and the inset the VDOS for P_M. The bottom right graph gives the HisM202 dihedral (red line) with the P_M-HOMO energy (bars) in the time domain.

monomers are very similar, we observe a delocalized HOMO (as one would expect from an exciton dimer-model). HOMO−LUMO photoexcitation of P at specific geometries will thus yield an excited state with strong CT character. We find both $P_L^+P_M^-$ and $P_L^-P_M^+$ CT characters to be present at room temperature as well as a delocalized pure exciton state P*. Comparing the relative HOMO−LUMO gap of $P_L^+P_M^-$ and $P_L^-P_M^+$ transitions, we find, in agreement with Stark experiments,[6] that $P_L^-P_M^+$ is the highest energy CT transition of the P absorption band. (See SI-3 of the Supporting Information for further comments.)

The thermal rearrangement of electron density over P opens the possibility to correlate electronic structure with distinct conformational dynamics, that is, to find the normal modes of P that couple to orbital localization. Fourier transform of the velocity autocorrelation function of the trajectories gives a

dx.doi.org/10.1021/jz201695p | J. Phys. Chem. Lett. 2012, 3, 694–697

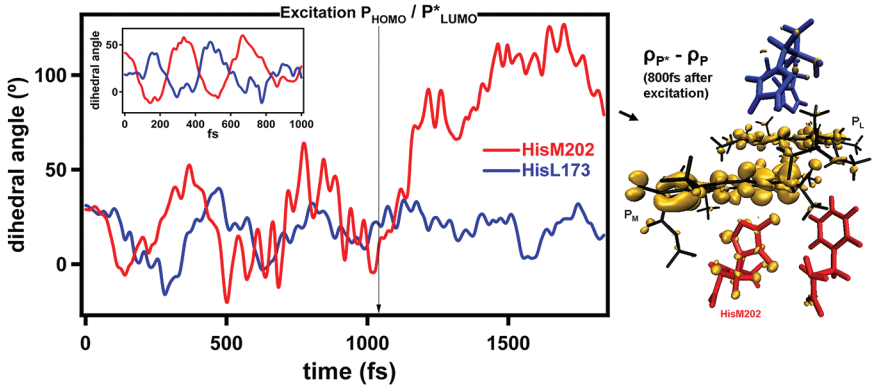

Figure 3. HisM202 (red line) and symmetry related HisL173 (blue line) dihedral angles representing the rotation of the histidine rings around the coordination Mg−Nτ axis as a function of time. (See also Figure 1, right bottom.) The arrow indicates the time step where we switch from ground state to excited state (ROKS) dynamics. In the inset for comparison, we show the same structural parameters along a different ground state trajectory. The right figure shows the positive values of the difference between the P* and P electron density ($\rho^{P*} - \rho^{P}$) at the end of the ROKS dynamics.

vibrational density of states that shows two distinct maxima at low frequencies, ∼50 and ∼100 cm^{-1} (Figure 2, gray shading in top graphs). To assign the peaks and resolve the appropriate conformational dynamics, we performed additional Fourier transforms of the velocity autocorrelation function of different components of the model and of individual structural parameters (e.g., dihedral angles and bond distances). The lowest frequency peak at ∼50 cm^{-1} is well-resolved in terms of the out-of-plane acetyl motion that couples strongly to the HisL168 imidazole ring dynamics through hydrogen-bond interaction (Figure 1, left top and Figure 2, blue lines). This is the characteristic vibrational coordinate of the mode, which is biased toward the P_L dimer half also absorbing at this frequency. (See Figure 2, middle top inset, where we consider the contribution of the two dimer halves separately.) A normal-mode analysis confirms the idea that the ∼50 cm^{-1} mode is dominated by collective motion of the P_L dimer half and the immediate protein environment. (See SI-4 and Movie 2 in the Supporting Information.) To correlate the vibrational coordinate with the electronic structure, we take the energies of the HOMO and HOMO-1 along the trajectory, and depending on the localization of these orbitals, we associate them with either the P_L or P_M dimer half. (See SI-5 in the Supporting Information for details.) The left bottom graph of Figure 2 shows the correlation between the P_L-HOMO energy (bars) and the hydrogen bond distance from the P_L-acetyl to the HisL168 with a computed Pearson correlation coefficient (ρ_c) $\rho_c = 0.64$; at minimum distance, the hydrogen bond is strongest and stabilizes the P_L-HOMO energy.

Equally pronounced in the total vibrational density of states, we find a peak at ∼100 cm^{-1} that is mostly localized on the P_M half of the dimer (Figure 2; inset, red line). Analysis of the structural dynamics showed an intriguing anticorrelated rotation of the two axial histidines with respect to the coordination Mg−N_τ axis (ρ_c= −0.81, illustrated by the inset in Figure 3; left top) expressed in terms of dihedral angles (Figure 1 inset; right bottom). Calculations of covariance between the L- and M-side axial histidines confirm this behavior, yielding negative values a factor of 2 to 4 larger than the negative covariance between the L and M bacteriochlorophyll planes. From the Fourier analysis, we find both dihedral angles to contribute to the 100 cm^{-1} mode, with the M-side dihedral showing larger amplitude (Figure 2, top right, red lines). The normal-mode analysis clearly confirms this picture; the modes around ∼100 cm^{-1} contain an anticorrelated rotation of the axial histidines with respect to the Mg−N_τ axis, the amplitude being larger on the M-side (Movie 3 in the Supporting Information). We conclude that the characteristic vibrational coordinate of the 100 cm^{-1} mode involves mostly the P_M dimer half and the axial rotation of the HisM202. The bottom right graph of Figure 2 shows the dihedral angle of HisM202 (red line) with the energy of the P_M-HOMO (bars) along the trajectory. Minima at 0, 350, and 700 fs in the energy of the P_M-HOMO correspond to maxima in the dihedral angle, revealing that these quantities are anticorrelated (ρ_c = −0.50). (See SI-6 in the Supporting Information for further comments.) The ground-state multidimensional configurational space along which the relative energies of P_L and P_M are modulated is thus essentially given by two collective coordinates with well-defined frequencies (∼50 and ∼100 cm^{-1}). Displacements along these coordinates change the localization of the frontier orbitals.

To explore the dynamical behavior in the excited state (P*), we perform a molecular dynamics simulation based on the restricted open-shell Kohn−Sham (ROKS) approach[12] starting from the previously equilibrated ground-state trajectory. By comparing the ground-state and the ROKS trajectories, we observe that there is a distinct conformational change induced by the photoexcitation. This is illustrated in Figure 3, showing the dihedral angles of the rotation of the axial histidines around the Mg−N_τ axis. In the ground state, we find a striking negative covariance between the rotations of the two histidines. (See also the inset in Figure 3.) After photoexcitation, the dihedral angle of HisM202 (red line), which was found to be characteristic of the vibrational coordinate of the 100 cm^{-1} mode (Movie 3 in the Supporting Information), increases from an average of ∼25° in the ground state to ∼80° in P* and the negative covariance is lost. The vibrational coordinate of the 50 cm^{-1} mode is not affected upon photoexcitation. We conclude that upon photoexcitation, P* couples selectively to the ∼100 cm^{-1} mode, which we propose is the same mode seen in resonance Raman studies (96 cm^{-1}),[14] in femtosecond absorption spectroscopy (94 cm^{-1}),[3] and possibly hole-burning studies (∼150 cm^{-1}).[4]

Independently, we verify how the HOMO energy varies with a distortion along the 100 cm^{-1} normal mode by performing single-point calculations corresponding to dihedral angle values

dx.doi.org/10.1021/jz201695p | J. Phys. Chem. Lett. 2012, 3, 694−697

of 5° and 50°. This gives a HOMO energy change of 0.1 eV and orbital localization from one dimer half to the other. (See SI-7 and Figure SI-7 in the Supporting Information.)

To check the effect of the dynamical evolution in the excited state on the electron density distribution, we consider the difference between the excited-state and ground-state electron density at selected snapshots along the ROKS dynamics. In Figure 3 (right), we plot the positive values of $\rho^{P*} - \rho^{P}$. We observe that electron density moves from P_L to P_M and onto the HisM202 in agreement with experimental findings that P* is dominated by a $P_L^+P_M^-$ CT character. (See also SI-8 in the Supporting Information.)[6,15] From the Moser–Dutton simplification, distance, rather than free energy ($-\Delta G$) and reorganization energy (λ), is the rate-defining variable in most biological electron-transfer reactions.[16,17] In the bacterial RC, where competing electron-transfer pathways have similar distances, the reaction coordinate, as identified in this work, displaces electron density asymmetrically, possibly increasing the electronic coupling with one (B_A) of the two accessory bacteriochlorophyll. Additional investigations with an extended model including the electron acceptor are needed to support this suggestion.

In conclusion, the ground-state electron density is continuously redistributed by thermally excited low-frequency collective modes (50 and 100 cm^{-1}) that tune the respective dimer halves energies and induce the thermal broadening of P. Upon photoexcitation, the excited-state P* couples selectively to the 100 cm^{-1} mode that lowers the P_M dimer half energy and effectively removes the barrier for charge separation, initiating a directional displacement of electron density that leads to a $P_L^+P_M^-$ intermediate. This insight is an important step forward in the development of biomimetic systems inspired by a mechanistic understanding of natural photosynthesis.

■ ASSOCIATED CONTENT

Supporting Information

Methods and computational details; spatial distribution of the HOMO along the AIMD trajectory; additional discussion on P absorption band; normal mode analysis; discussion on the formation of the first photoproduct; and LUMO as a function of a displacement along the 100 cm^{-1} normal mode. Three movies are available: HOMO and LUMO localization, normal mode at ∼50 cm^{-1}, and normal mode at ∼100 cm^{-1}. This material is available free of charge via the Internet at http://pubs.acs.org.

■ AUTHOR INFORMATION

Corresponding Author

*E-mail: f.buda@chem.leidenuniv.nl.

Notes

The authors declare no competing financial interest.

■ ACKNOWLEDGMENTS

The use of supercomputer facilities was sponsored by The Netherlands National Computing Facilities Foundation (NCF), with financial support from The Netherlands Organization for Scientific Research (NWO). We acknowledge financial support from the BioSolar Cells program (project number C1.9). Huub Adriaanse is acknowledged for his contribution during the Bachelor Internship.

■ REFERENCES

(1) Novoderezhkin, V.; Yakovlev, A.; van Grondelle, R.; Shuvalov, V. Coherent Nuclear and Electronic Dynamics in Primary Charge Separation in Photosynthetic Reaction Centers: A Redfield Theory Approach. *J. Phys. Chem. B* **2004**, *108*, 7445–7457.

(2) Vos, M. H.; Jones, M. R.; Hunter, C. N.; Breton, J.; Martin, J. L. Coherent Nuclear Dynamics at Room Temperature in Bacterial Reaction Centers. *Proc. Natl. Acad. Sci. U.S. A.* **1994**, *91*, 12701–12705.

(3) Rischel, C.; Spiedel, D.; Ridge, J. P.; Jones, M. R.; Breton, J.; Lambry, J. C.; Martin, J. L. Low Frequency Vibrational Modes in Proteins: Changes Induced by Point-Mutations in the Protein-Cofactor Matrix of Bacterial Reaction Centers. *Proc. Natl. Acad. Sci. U.S.A.* **1998**, *95*, 12306–12311.

(4) Reddy, N. R. S.; Kolaczkowski, S. V.; Small, G. J. A Photoinduced Persistent Structural Transformation of the Special Pair of a Bacterial Reaction Center. *Science* **1993**, *260*, 68–71.

(5) Holzapfel, W.; Finkele, U.; Kaiser, W.; Oesterhelt, D.; Scheer, H.; Stilz, H. U.; Zinth, W. Initial Electron-Transfer in the Reaction Center from Rhodobacter Sphaeroides. *Proc. Natl. Acad. Sci. U.S.A.* **1990**, *87*, 5168–5172.

(6) Moore, L. J.; Zhou, H.; Boxer, S. G. Excited-State Electronic Asymmetry of the Special Pair in Photosynthetic Reaction Center Mutants: Absorption and Stark Spectroscopy. *Biochemistry* **1999**, *38*, 11949–11960.

(7) Daviso, E.; Prakash, S.; Alia, A; Gast, P.; Neugebauer, J.; Jeschke, G.; Matysik, J. The Electronic Structure of the Primary Electron Donor of Reaction Centers of Purple Bacteria at Atomic Resolution As Observed by Photo-CIDNP 13C NMR. *Proc. Natl. Acad. Sci. U. S. A.* **2009**, *106*, 22281–22286.

(8) Johnson, E. T.; Mu, F.; Nabedryk, E.; Williams, J. C.; Allen, J. P.; Lubitz, W.; Breton, J.; Parson, W. W. Electronic and Vibronic Coupling of the Special Pair of Bacteriochlorophylls in Photosynthetic Reaction Centers from Wild-Type and Mutant Strains of Rhodobacter Sphaeroides. *J. Phys. Chem. B* **2002**, *106*, 11859–11869.

(9) Alia, Wawrzyniak, P. K.; Janssen, G. J.; Buda, F.; Matysik, J.; de Groot, H. J. M. Differential Charge Polarization of Axial Histidines in Bacterial Reaction Centers Balances the Asymmetry of the Special Pair. *J. Am. Chem. Soc.* **2009**, *131*, 9626–9627.

(10) Wawrzyniak, P. K.; Beerepoot, M. T. P.; de Groot, H. J. M.; Buda, F. Acetyl Group Orientation Modulates the Electronic Ground-State Asymmetry of the Special Pair in Purple Bacterial Reaction Centers. *Phys. Chem. Chem. Phys.* **2011**, *13*, 10270–10279.

(11) Car, R.; Parrinello, M. Unified Approach for Molecular Dynamics and Density-Functional Theory. *Phys. Rev. Lett.* **1985**, *55*, 2471–2474.

(12) Marx, D.; Hütter, J. *Ab Initio Molecular Dynamics: Basic Theory and Advanced Methods*; Cambridge University Press: Cambridge, U.K., 2009.

(13) Cohen Stuart, T.; van Grondelle, R. Multipulse Spectroscopy on the Wild-Type and YM210W Bacterial Reaction Centre Uncovers a New Intermediate State in the Special Pair Excited State. *Chem. Phys. Lett.* **2009**, *474*, 352–356.

(14) Cherepy, N. J.; Shreve, A. P.; Moore, L. J.; Boxer, S. G.; Mathies, R. A. Temperature Dependence of the Q_y Resonance Raman Spectra of Bacteriochlorophylls, the Primary Electron Donor, and Bacteriopheophytins in the Bacterial Photosynthetic Reaction Center. *Biochemistry* **1997**, *36*, 8559–8566.

(15) Shuvalov, V.; Yakovlev, A. Coupling of Nuclear Wavepacket Motion and Charge Separation in Bacterial Reaction Centers. *FEBS Lett.* **2003**, *540*, 26–34.

(16) Moser, C. C.; Keske, J. M.; Warncke, K; Farid, R. S.; Dutton, L. P. Nature of Biological Electron Transfer. *Nature* **1992**, *355*, 796–802.

(17) Creighton, S.; Hwang, J. K.; Warshel, A; Parson, W. W.; Norris, J. Simulating the Dynamics of the Primary Charge Separation Process in Bacterial Photosynthesis. *Biochemistry* **1988**, *27*, 774–781.